Plasmonics (2023) 18:1725–1734
https://doi.org/10.1007/s11468-023-01885-y

RESEARCH

Titanium Dioxide-2D Nanomaterial Based on the Surface Plasmon Resonance (SPR) Biosensor Performance Signature for Infected Red Cells Detection

Yesudasu Vasimalla[1] · Himansu Shekhar Pradhan[2] · Rahul Jashvantbhai Pandya[3] · Kayam Saikumar[4] · Twana Mohammed Kak Anwer[5] · Ahmed Nabih Zaki Rashed[6,7] · Md. Amzad Hossain[8]

Received: 27 April 2023 / Accepted: 17 May 2023 / Published online: 30 May 2023

Abstract

This paper presents a performance signature of a surface plasmon resonance (SPR) sensor for infected red blood cells (RBCs) detection using titanium dioxide (TiO_2)-2D nanomaterial-based structure. There is a substantial deviation between RBCs with and without *Plasmodium falciparum* infection, which can be represented in refractive indices showing the disease's diagnosis. For the detection process, the proposed structure is made up by Kretschmann setup with silver (Ag), TiO_2, and 2D nanomaterials. Here, Ag excites the surface plasmons on prism surface as well as provide sharp resonance dip that lead to better resolution and quality. Likewise, TiO_2 has admirable electronic and optical properties, including high photocatalytic activity and chemical stability, and is placed between Ag and 2D nanomaterial s for increased sensitivity. Different nanomaterials, MXene, graphene, black phosphorus, and molybdenum disulfide (MoS_2), are used to improve the sensor's efficiency. Sensing parameters are measured by exploiting the transfer matrix method. Initially, an impact of TiO_2 in the SPR sensor is presented, concluding that 18% of sensitivity is improved after adding TiO_2 to the conventional structure. Moreover, utilization of 2D nanomaterial in the proposed sensor is observed, resulting that the respected 2D materials are improved the sensitivity by 11%, 4%, 10%, and 34% compared to the TiO_2-based sensor. The maximum achieved parameters are a sensitivity of 475.71°/RIU, a quality factor of 236.67 RIU^{-1}, and detection accuracy of 5.95, which are improved extremely compared to existing works.

Keywords Biosensor · Kretschmann configuration · Red blood cells · Surface plasmon resonance · Transfer matrix method

Introduction

Malaria caused by the *Plasmodium* parasite, has become a problematic illness that severely affects human beings. It is also a main cause of the high death rate in pervasive nations among both children and adults. In addition, 44% of individuals on the earth are at risk of contracting the disease [1]. Infections of "Falciparum, ovale, malariae, vivax, and knowlesi" are several *Plasmodium* that can cause malaria. Among these, *P. falciparum* infections are the main contributor to mortality from malaria. Mosquitoes transmit the parasite *Plasmodium*. Because they often bite between sunset and daybreak, these mosquitoes are referred to as "night-biting" mosquitoes. The parasite enters the bloodstream and moves to the liver when an infected mosquito bites a person. Before returning to circulation, it grows in the liver for several days to weeks. At this stage, symptoms start to appear, necessitating immediate medical attention [2–5]. After the hepatocytes are injured, the parasites enter the bloodstream as merozoites, attacking the red blood cells (RBCs), and then begin an intraerythrocytic cycle [6–9]. This cycle results in structural and metabolic changes to RBCs. The ring phase that initiates this cycle is triggered by merozoites interacting with RBCs and is followed by mononuclear trophozoites. Moreover, trophozoites can transform into schizonts, which are multinucleated cells, when hemoglobin is broken down, and hemozoin is generated [10]. In the "intraerythrocytic series," healthy erythrocytes display a homogeneous distribution of refractive index across the cell's cytoplasm compared to rotting erythrocytes [11]. There is a significant difference in refractive index between infected and uninfected red blood cells, and it can be used as a critical indicator when diagnosing malaria [12]. An optical

Extended author information available on the last page of the article

microscope analysis of a blood smear is the primary method to determine whether a patient has malaria. The operation requires a skilled and experienced laboratory professional, and it takes time for the results to be returned [13]. The other two diagnostic techniques available exist for malaria determination, and they are "polymerase chain reaction (PCR) and rapid diagnostic testing (RDT)." Due to many problems with their sensitivity, specificity, and more expensive, these approaches are less effective [14]. As a result, a simple and accurate diagnosis system is required for controlling and treating the disease and avoiding hitches and transience [15].

Due to its characteristics, including reflectance, light wave absorption, and transmittance, which fluctuate according to the environment, optical biosensors currently dominate the rapidly advancing technology. Also, the sensors can accurately detect various ailments using various biomedical devices [16]. They also provide superior sensitivity and precision in relation to the medium RI. In recent years, surface plasmon resonance (SPR)-based sensors have become famous and emergent compared to other sensors for optical sensing due to their remarkable progress in manufacturing expertise [17]. It is utilized to identify variations in the RI of biological samples and chemical analytes that are directly related to the structure of the sensor [18]. The SPR sensor operates under the attenuated total reflection (ATR) method that is also used to observe changes in a layer's RI. Also, the ATR approach makes use of the total internal reflection (TIR) principle, which creates the surface plasmon wave (SPW) on the metal–dielectric interface [19]. At the very least, the incident light that travels through the ATR crystal is reflected off while the inside surface makes contact with the detecting zone. In order to produce a transient electromagnetic wave that propagates along the metal and dielectric contact, SPR needs optical excitation [20]. The chemical reaction does the changes in the biomolecules' concentration and the sensing RI that lead to changes in the SPW's propagation constant. Consequently, corresponding changes occur in the SPR resonance angle [21].

Hence, this method can be used to perceive different analyte features in the sensing zone. For a long time, gold (Au) and silver (Ag) are primarily used as metallic layers, which are coated over the prism's surface to excite surface plasmons due to optical properties like high sensitivity, SPR ratio, and less optical damping. However, Ag offers a sharp resonance dip that leads to good precision and resolution, whereas Au struggles with a broader curve and has poor molecule binding capabilities [4, 22]. Tough Ag provides a sharp resonance dip but suffers more susceptible to oxidation; therefore, to overcome the oxidation problem, the nanostructured semiconductor metal oxide titanium dioxide (TiO_2) is placed ahead of Ag metal film because of its exceptional properties like a broadband gap (3.2 eV for anatase and 3.0 eV for rutile), a strong absorbability, excellent chemical stability, and a high RI (i.e., 2.5 for anatase and 2.7 for rutile). Due to the aforementioned traits, the TiO_2 layer is added to the interface to produce field confinement and enhancement, which is advantageous for sensitivity improvement [4–6, 23]. Furthermore, two-dimensional (2D) nanomaterial is considered over the TiO_2 to enhance the sensor's accuracy and efficiency. MXene, graphene, black phosphorus (BP), and molybdenum disulfide (MoS_2) are popular 2D family nanomaterials. A wide range of applications has been made possible by the combination of properties that make MXenes unique [7–9]. These properties include high electrical conductivity, the mechanical properties of transition metal carbides/nitrides, functionalized surfaces that make MXenes' hydrophilic and prepared to bond to different species, high negative zeta-potential, which enables stable colloidal solutions in water, and effective absorption of electromagnetic waves [9, 24]. A substance made of sp^2 carbon layers with an atomically thin structure and a honeycomb lattice is known as graphene. Graphene has received the most research attention in the 2D family over the past 10 years due to its many remarkable properties, including its large surface area, high charge-carrier mobility, high thermal conductivity, high optical activity, high mechanical strength, and low Young's modulus [25]. It's fascinating to note that 2D black phosphorus has a distinctive wrinkled structure, a high hole mobility of up to 1000 $cm^2\ V^{-1}\ s^{-1}$, excellent mechanical properties, tunable band structures, and anisotropic thermal, electrical, and optical properties, all of which contribute to its fantastic prospects in device applications [26]. MoS_2 has two characteristics as a result of its model: a hexagonal structure made up of covalently bound S-Mo-S atomic layers and a "van der Waals" contact between adjacent layers that can be used for gas sensing. It also has a thermal conductivity of 131 $Wm^{-1}\ k^{-1}$ at ambient temperature [6–8, 26]. Therefore, this study considers the proposed novel structure that is comprised of six layers, such as BK7, Ag, TiO_2, 2D nanomaterial, and sensing medium, for the detection of infected red cells. The reason for this is that there is a substantial deviation between RBCs with and without *Plasmodium falciparum* infection, which can be represented in refractive indices showing the disease's diagnosis.

Fabrication Process

The BK7 prism must first be thoroughly cleaned with a piranha solution for 1 h at 80 °C to get rid of any impurities or flaws. After that, it needs to be air-dried and rinsed with distilled water. The prism must then be placed within the electron beam evaporator with a fundamental vacuum of 6×10^{-6} Torr. Then, a thin coating (1 or 2 nm) of chromium (99.95% purity) must be coated over the prism surface by electron beam evaporation in order to increase the Ag

adhesion on the prism surface. Then, the conditions can be tuned to be voltage of 8.5 kV, current of 45 mA, and deposition rate of 0.5 $\dot{A}/s$ for creating an Ag (99.99% purity) layer [27]. A quartz crystal monitor is capable of controlling the layer thickness and deposition rate. The TiO_2 layer can then be placed on top of the Au film. TiO_2 can be created by dissolving 0.1 N of titanium tetra isopropoxide in 20 ml of ethanol solution after 30 min of constant stirring. After that, we add a few drops of distilled water to form the dispersion medium. Twenty minutes was spent with the object in the ultrasonic bath [28]. It is then necessary to place a layer of 2D nanomaterial on top of the TiO_2. Researchers in [29] have a thorough discussion and provide specific information about the synthesis of all 2D nanomaterials. In order to identify red blood cells, a sensor chip is lastly placed on the rotating stage of the experiment setup [30].

Theory and Methodology

The current section presents the design parameters, mathematical models, and equations to measure the sensor's performance.

Design Parameters

Figure 1 shows the schematic structure of the proposed sensor for red blood cell detection. The structure is made up of the Kretschmann configuration, which has the advantage of high spectral signal-to-noise ratio by allowing the measurement of directional Raman signals from thin metal films [30]. BK7 glass is utilized for light-coupling with a refractive index (RI) of 1.515 at 633 nm wavelength (λ), where it can provide the least amount of Kerr effect [31]. To excite surface plasmons (SPs) at the prism-metal interface, a metal film of silver (Ag) is placed over the prism's surface with an RI of 0.059 + 4.243i [32]. Furthermore, TiO_2 is comprised over the Ag layer to improve the capability of molecular binding, having the RI of 2.5836 [33]. Moreover, 2D nanomaterial is paced on the TiO_2 to preclude the susceptibility to oxidization and improve sensor's efficiency. For this study, different 2D nanomaterials are considered such as MXene, graphene, BP, and MoS_2 with RI of 2.38 + 1.33i [34], 3 + 1.1491i [35], 3.5 + 0.01i [36], and 5.0947 + 1.2327i [37], and thickness of 0.993, 0.34, 0.53, and 0.65 nm, respectively. Finally, the sensing region that consists of red blood cells concentration is comprised over 2D nanomaterial. Four RBCs are considered for this study, and they are normal RBC (NRBC), ring RBC (RRBC), trophozoite phase RBC (TRBC), and schizont phase RBC (SRBC) with RI of 1.402, 1.395, 1.383, and 1.373, respectively [38].

Methodology

This study has investigated the sensor's performance by employing the transfer matrix method (TMM) with Fresnel model analysis of multilayer reflection theory. In this event, the minimum reflectance intensity (R_{min}) of SPR curve occurs at the resonance condition, while the propagation constant (PC) of electromagnetic wave (k_x) is equal to PC of the wave vector of surface plasmons (k_{spw}). The equaling mathematical expressions are mentioned in Eqs. (1) and (2) [39]. Furthermore, the resonance angle (θ_{SPR}), which is an angle where R_{min} is attained, can be evaluated through Eq. (3) [40], where n_p, n_{Au}, n_{TiO2}, and n_S are represented the RIs of the prism, Ag,TiO_2, and sensing medium, respectively.

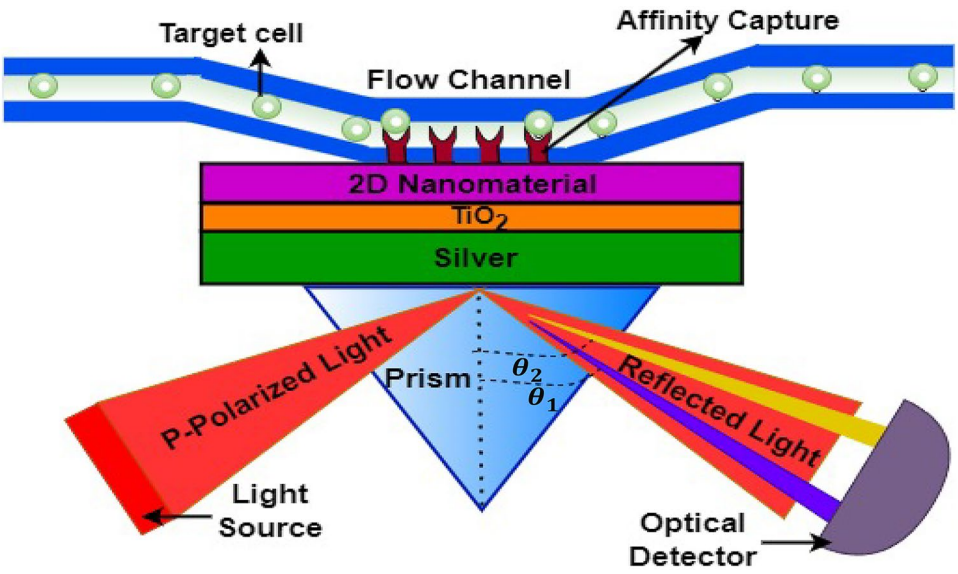

Fig. 1 Schematic structure of the proposed sensor for red blood cell detection

$$k_x = k_{SPW} \tag{1}$$

$$\frac{2\pi}{\lambda_{633}}\left(n_p \sin\theta\right) = \frac{2\pi}{\lambda_{633}}\sqrt{\frac{n_{Ag}^2 n_{TiO2}^2}{n_{Ag}^2 + n_{TiO2}^2}} \tag{2}$$

$$\theta_{SPR} = \left(\sin\sqrt{\frac{n_{Ag}^2 n_s^2}{n_p^2\left(n_{Ag}^2 + n_s^2\right)}}\right)^{-1} \tag{3}$$

Moreover, the study analyzes reflectance intensity for the SPR sensor by exploiting the angular interrogation technique, where reflectance measures with respect to an angle. Therefore, the SR curve for the study plots between the reflectance intensity (R_p) and the incidence angle. The mathematical representations for measuring the R_p and reflection coefficient (r_p) are made known in Eqs. (4) and (5), respectively [41].

$$R_p = r_p r_p^* = \left|r_p\right|^2 \tag{4}$$

$$r_p = \frac{\left(Z_{11} + Z_{12} m_N\right) - \left(Z_{21} + Z_{22} m_N\right)}{\left(Z_{11} + Z_{12} m_N\right) + \left(Z_{21} + Z_{22} m_N\right)} \tag{5}$$

where m_N represents a description of the transverse RI for the corresponding N^{th} layer, and numerically calculate by using Eq. (6) [42].

$$m_k = \left[\frac{\mu_k}{\varepsilon_k}\right]^{1/2} \cos\theta_k = \sqrt{\frac{\varepsilon_k - \left(n_p \sin\theta\right)^2}{\varepsilon_k^2}} \tag{6}$$

Furthermore, Eq. (7) demonstrates the properties matrix of the SPR sensor combined structure (Z_{if}) for P-polarized incident light [32], where β_k represents the arbitrary stage constant for *k*th layer and numerically expressive in Eq. (8) [43].

$$Z_{if} = \left[\prod_{k=2}^{N-1}\begin{pmatrix}\cos\beta_k & -i\sin\beta_k \\ -in_k \sin\beta_k & \cos\beta_k\end{pmatrix}\right]_{if} = \begin{bmatrix}Z_{11}Z_{12} \\ Z_{21}Z_{22}\end{bmatrix} \tag{7}$$

$$\beta_k = \frac{2\pi}{\lambda} n_k \cos\theta_k \left(z_k - z_{k-1}\right) = \frac{2\pi}{\lambda} d_k \sqrt{\varepsilon_k - \left(n_p \sin\theta\right)^2} \tag{8}$$

Here, z_k and θ_k express the wave impedance and input angle, at *k*th layer, respectively, and mathematically presented in Eqs. (9) and (10), respectively [44], where ε_k, μ_k, and d_k are represented the permittivity, permeability, and thickness of *k*th layer, respectively.

$$z_k = \frac{k_x m_k \cos\theta_k}{\left(2\pi c/\lambda_{633}\right)\varepsilon_k^2} \tag{9}$$

$$\theta_k = \left(\cos\sqrt{1 - \left(m_{k-1}/m_k\right)(\sin\theta)^2}\right)^{-1} \tag{10}$$

The obtained mathematical expression for calculating the reflectivity of the suggested sensor, which includes five layers of structures, is displayed below Eq. (11), obtained after all the defined parameters have been substituted in Eq. (4) [45].

$$R_{12345} = \left|r_{12345}\right|^2 = \left|\frac{r_{12} + r_{2345}\, e^{2ik_2 d_2}}{1 + r_{12} r_{2345}\, e^{2ik_2 d_2}}\right|^2 \tag{11}$$

$$r_{2345} = \frac{r_{23} + r_{3456}\, e^{2ik_3 d_3}}{1 + r_{23} r_{3456}\, e^{2ik_3 d_3}}, r_{345} = \frac{r_{34} + r_{456}\, e^{2ik_4 d_4}}{1 + r_{34} r_{456}\, e^{2ik_4 d_4}}, r_{12} = \frac{\varepsilon_2/k_2 - \varepsilon_1/k_1}{\varepsilon_2/k_2 + \varepsilon_1/k_1},$$
$$r_{23} = \frac{\varepsilon_3/k_3 - \varepsilon_2/k_2}{\varepsilon_3/k_3 + \varepsilon_2/k_2}, r_{34} = \frac{\varepsilon_4/k_4 - \varepsilon_3/k_3}{\varepsilon_4/k_4 + \varepsilon_3/k_3}, \; r_{45} = \frac{\varepsilon_5/k_5 - \varepsilon_4/k_4}{\varepsilon_5/k_5 + \varepsilon_4/k_4}$$

where r_{12}, r_{23}, r_{34}, and r_{45} are well defined the reflected amplitudes from 1–2, 2–3, 3–4, and 4–5 layers, respectively, and d_m denotes thickness of each layer ($m = 2, 3, 4, 5$).

Sensing Performance Parameters

In this study, we measure three basic and important sensing parameters, such as sensitivity, quality factor (QF), and detection accuracy (DA), to showing the impact of the proposed SPR sensor. Sensitivity refers to the ratio of change in the resonance angle ($\nabla\theta_{res}$) to the change in the RI (∇n). The enhanced sensitivity of an SPR sensor for a minute amount of biomolecule concentration variation, it demonstrates shows that it can incredibly detect minute structural alterations. Similarly, QF refers as the ratio of sensitivity to full-width-half-maximum (FWHM), where FWHM is the SPR curve's width at 50% of maximum reflectance intensity. Finally, DA refers as the ratio of $\nabla\theta_{res}$ to FWHM. The improved performance of QF and DA demonstrates product quality, noise influence, and sensor accuracy. The mathematical expressions to compute the defined parameters are shown in Eqs. (12)–(14) [31, 43].

$$\text{Sensitivity} = \frac{\nabla\theta_{res}}{\nabla n}\ (^\circ/\text{RIU}) \tag{12}$$

$$\text{Quality Factor (QF)} = \frac{S}{(\text{FWHM})}\ (\text{RIU}^{-1}) \tag{13}$$

$$\text{Detection Accuracy (DA)} = \frac{\nabla\theta_{res}}{\text{FWHM}} \tag{14}$$

Results and Discussions

In the first part, the impact of TiO_2 in the structure is shown by comparing the performance between conventional (prism-Ag-sensing) and TiO_2-based (prism-Ag-TiO_2-sensing) structures. Figure 2a, b show the reflectance curves with respect to an angle for normal and infected RBCs using conventional and TiO_2-based structures, respectively. For Fig. 2a, we have considered to Ag thickness of 40 nm because < 40 nm is not generated the SPR curve, whereas TiO_2 thickness of 1 nm is taken between Ag and sensing layer for Fig. 2b; the asymmetrical property is observed in Fig. 2, due to fluctuations in the SPW's penetration length and damping effect [33, 36]. Figure 2a generates the resonance angles of 77.80, 76.6, 74.6, and 73.09° for NRBC, RRBC, TRBC, and SRBC, respectively. Sensitivity is measured using Eq. (12) and obtained sensitivities are 171.43, 168.42, and 162.41°/RIU for infected cells of RRBC, TRBC, and SRBC, respectively. Similarly, Fig. 2b shows the resonance angles of 79.1, 77.68, 75.53, and 73.96° for NRBC, RRBC, TRBC, and SRBC, respectively. Obtained sensitivities are 202.86, 187.89, and 177.24°/RIU for infected cells of RRBC, TRBC, and SRBC, respectively. The impact of TiO_2-based sensor is that it improves the sensitivity by 18% compared to the conventional sensor. Figure 3 presents the graphical representation of obtained resonance angles for conventional and TiO_2-based sensors. It demonstrates how the desired direction of the SPR resonance shift moves, proving that the suggested sensor satisfies the SPR property [35].

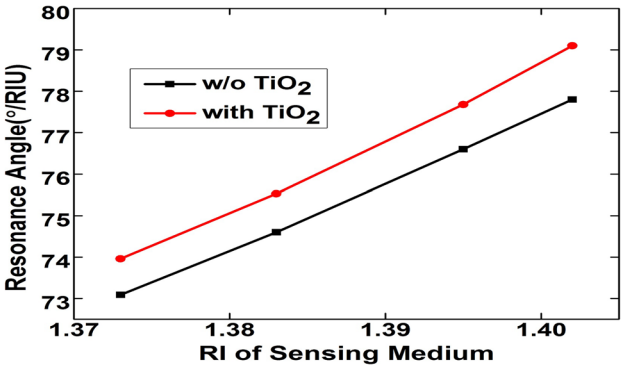

Fig. 3 Obtained resonance angles with respect to a sensing RI for conventional and TiO_2-based sensors

The literature identified that the sensitivity and efficiency of the sensor can be improved by adding 2D nanomaterial to an SPR structure. Therefore, in the second part, the impact of 2D nanomaterial is presented by calculating and comparing

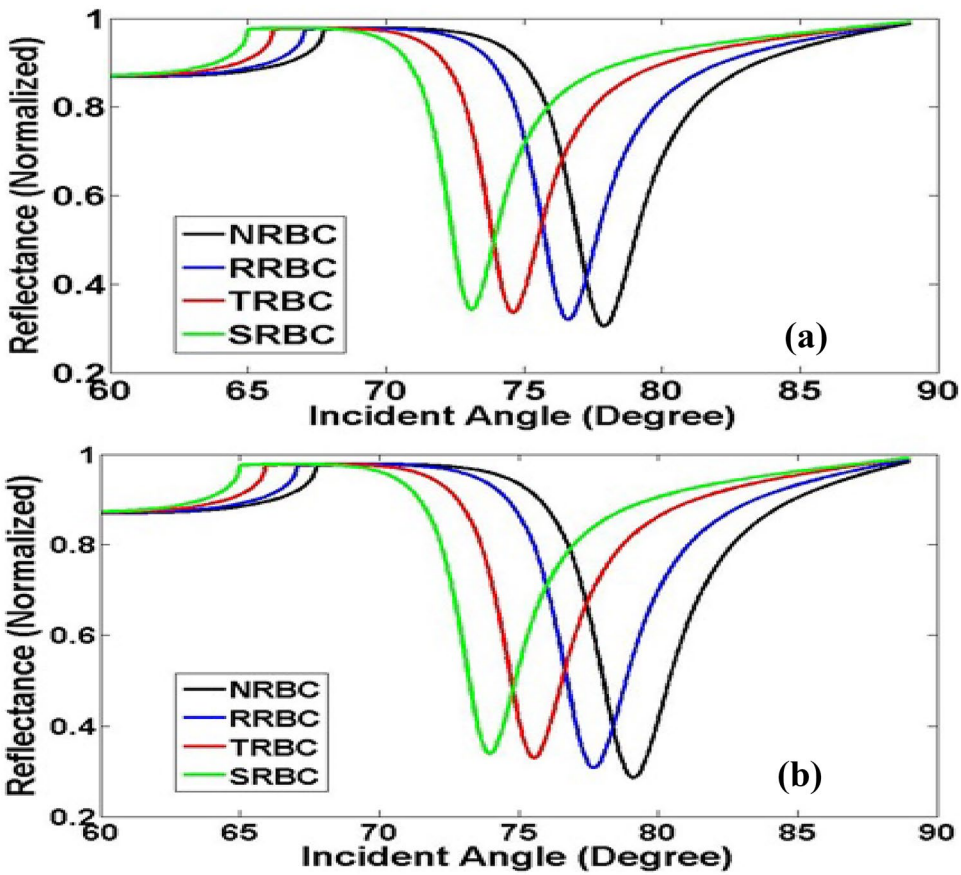

Fig. 2 Measuring reflectance with respect to an angle for normal and infected RBCs using **a** conventional, **b** TiO_2-based structures

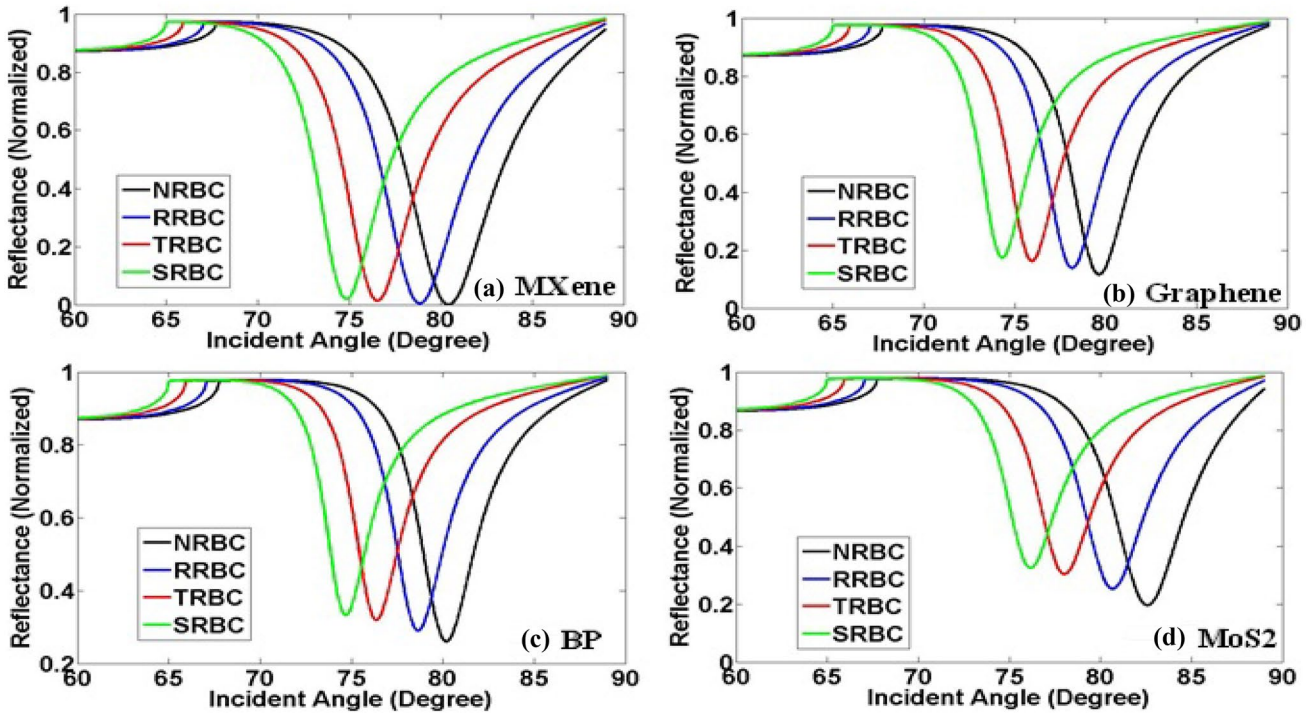

Fig. 4 Reflectance curves for normal and infected RBCs using different nanomaterial **a** MXene, **b** graphene, **c** BP, and **d** MoS_2

the performance of different 2D materials. Four 2D nanomaterials, such as MXene, graphene, BP, and MoS_2, are considered for the study. Figure 4 presents the reflectance curves for normal and infected RBCs using the considered nanomaterials, whereas Fig. 4a for MXene, Fig. 4b for graphene, Fig. 4c for BP, and Fig. 4a for MoS_2. In Fig. 4, the SPR curves' width are increased when compared to the TiO_2-based sensor because of the damping effect that increases by depositing several layers to the sensor [29]. The obtained resonance angles for respected normal and infected RBCs are 80.41, 78.84, 76.52, and 74.83° using MXene, 79.62, 78.14, 75.94, and 74.31 using graphene, 80.20, 78.64, 76.34, and 74.69° using BP, and 82.58, 80.67, 78.03, and 76.17° using MoS_2. For better understanding, the obtained resonance angles are reported in Table 1. Sensitivity for Fig. 4 is measured by applying Eq. (12) and reported in Table 2. The maximum sensitivity of 224.29, 211.43, 222.86, and 272.86°/RIU for respected, considered 2D materials improved the sensitivity of 11%, 4%, 10%, and 34%, respectively, compared to TiO_2-based sensor. This improvement happens as a result of their outstanding mechanical, optoelectrical, and penetration depth (PD) qualities [29]. The PD monitors the SPs' contact length in the transverse direction, which is sensitive because biomolecules are bonded to the sensing surface in order to detect the RI shift of the sensing medium [31]. The MoS_2 provided maximum sensitivity of 272.86°/RIU, which is 1.21, 1.29, and 1.22 times higher than MXene, graphene, and BP 2D materials, respectively. Therefore, with this study, we concluded that the prism-Ag-TiO_2-MoS_2-sensing structure, which is used for further investigation of the sensor, provides better performance compared to other 2D materials.

Furthermore, optimization of Ag thickness is obtained in this section using the iteration method. In this study, Ag thickness of 40 to 60 nm is varied with an interval of 5 nm while maintaining the constant thicknesses of TiO_2 and MoS_2 at 1 nm and 0.65 nm, respectively. The SPR property

Table 1 Measured resonance angles for considered 2D nanomaterials

Structure	Resonance angle (°)			
	MXene	Graphene	BP	MoS_2
NRBC	80.41	79.62	80.2	82.58
RRBC	78.84	78.14	78.64	80.67
TRBC	76.52	75.94	76.34	78.03
SRBC	74.83	74.31	74.69	76.17

Table 2 Measured sensitivities for considered 2D nanomaterials

Structure	Resonance angle (°)			
	MXene	Graphene	BP	MoS_2
NRBC	-	-	-	-
RRBC	224.29	211.43	222.86	272.86
TRBC	204.74	193.68	203.16	239.47
SRBC	192.41	183.10	190.00	221.03

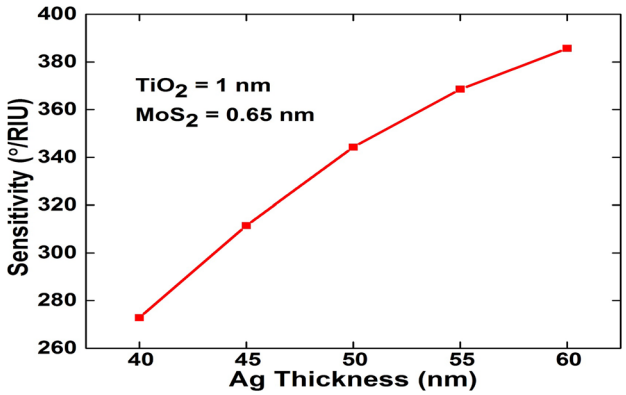

Fig. 5 Measured sensitivities with respect to Ag thickness for optimizing the layer thickness

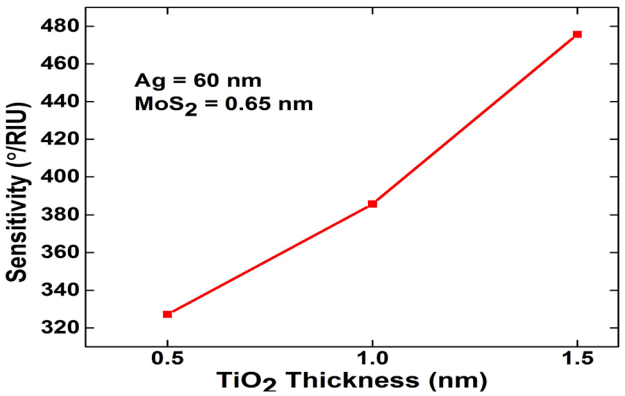

Fig. 6 Measured sensitivities with respect to TiO_2 thickness for optimizing the layer thickness

is not satisfied at an Ag thickness of > 60 nm. In the previous study, the maximum sensitivity is accomplished for the detection of RRBC. Therefore, we calculate the sensitivity for the detection of RRBC to optimize the Ag thickness. The obtained sensitivities are 272.86, 311.43, 344.29, 368.57, and 385.71 °/RIU for Ag thickness of 40, 45, 50, 55, and 60 nm, respectively. Figure 5 shows the graphical representation of obtained sensitivities with respect to Ag thickness, whereas Table 3 reported the resonance angles and sensitivity for NRBC and RRBC. Therefore, since it provides the maximum sensitivity, we concluded that the optimized thickness of Ag is 60 nm, which is used for further analysis of the study for the proposed SPR sensor.

Similarly, the optimization of TiO_2 thickness is presented in this section. For the event, TiO_2 thickness is varied from 0.5 to 1.5 nm with an interval of 0.5 nm, while keeping the constant thickness of Ag and MoS_2 at 60 and 0.65 nm, respectively. The SPR property is not satisfied at TiO_2 thickness of > 1.5 nm. The achieved sensitivities are 327.14, 385.71, and 475.71 °/RIU for TiO_2 thickness of 0.5, 1, and 1.5 nm, respectively. Figure 6 shows that obtained sensitivities with respect to TiO_2 thickness, whereas Table 4 noted the resonance angles and corresponding sensitivities. Therefore, this study witnessed that the optimized thickness of TiO_2 is 1.5 nm, where it achieves the maximum sensitivity, and the same thickness is used for further investigation.

Moreover, optimization of MoS_2 thickness for the proposed sensor is exhibited. Here, we consider MoS_2 thickness is S × 0.325, while keeping the constant thickness of Ag and TiO_2 at 60 and 1.5 nm, respectively, where S is number of MoS_2 layers that varied from 1 to 2.5 with an interval of 0.5. The SPR property is not satisfied at MoS_2 layers of > 2.5. The sensitivities of 320, 381.43, 475.71, and 294.29 °/RIU are achieved for MoS_2 layers of 1, 1.5, 2, and 2.5, respectively. The maximum sensitivity is furnished at S = 2; therefore, this study confirmed that the optimized thickness of MoS_2 is 0.65 nm. The graphical representation of furnished sensitivities are depicted in Fig. 7, whereas Table 5 noted the resonance angles and corresponding sensitivities.

After optimizing the thickness of Ag, TiO_2, and MoS_2 at 60, 1.5, and 0.65 nm, respectively, the SPR reflectance curves with respect to an angle are clarified for respected RBCs; the obtained resonance angles and sensing parameters, such as sensitivity, QF, and DA that are calculated using Eqs. (12)–(14) are reported in Table 5. The resonance angle of Fig. 8 is satisfied the SPR property.

The obtained resonance angles are 86.76, 83.43, 79.41, and 77.42° for respected RBCs. The obtained sensitivities are 475.71, 371.05, and 322.07; QF are 236.82, 210.82, and 205.14; DA are 1.66, 4.01, and 5.95 for infected RRBC, TRBC, and SRBC, respectively, where FWHM

Table 3 Resonance angle and sensitivity vs Ag thickness

Ag thickness (nm)	Resonance angle (°)		$\nabla\theta_{res}$(°)	Sensitivity (°/RIU)
	NRBC	RRBC		
40	82.58	80.67	1.91	272.86
45	83.34	81.16	2.18	311.43
50	83.98	81.57	2.41	344.29
55	84.44	81.86	2.58	368.57
60	84.79	82.09	2.71	385.71

Table 4 Resonance angle and sensitivity vs TiO_2 thickness

TiO_2 thickness (nm)	Resonance angle (°)		$\nabla\theta_{res}$(°)	Sensitivity (°/RIU)
	NRBC	RRBC		
0.5	83.25	80.96	2.29	327.14
1	84.79	82.09	2.7	385.71
1.5	86.76	83.43	3.33	475.71

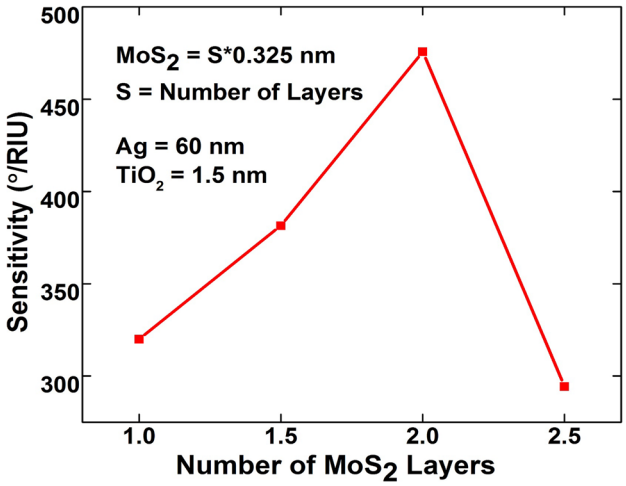

Fig. 7 Measured sensitivities with respect to MoS_2 thickness for optimizing the layer thickness

Table 5 Resonance angle and sensitivity vs MoS_2 thickness

TiO_2 thickness (nm)	Resonance angle (°)		$\nabla\theta_{res}$(°)	Sensitivity (°/RIU)
	NRBC	RRBC		
1	83.08	80.84	2.24	320
1.5	84.67	82	2.67	385.71
2	86.76	83.43	3.33	475.71
2.5	87.32	85.26	2.06	294.29

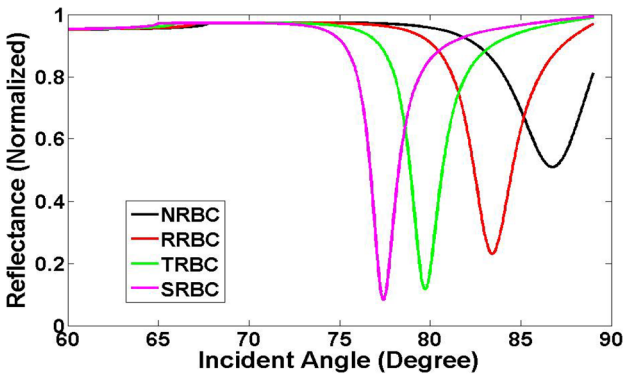

Fig. 8 Reflectance curves for normal and infected blood cells using the proposed structure

Table 6 Performance comparison between proposed and existing work

References	Sensitivity (°/RIU)	QF (RIU^{-1})	DA
Jia et al. [39]	165	-	-
Pal et al. [40]	156.33	-	0.64
Taya et al. [41]	103	-	-
Mudgal el al. [42]	194.12	16.04	0.27
Pal and Jha [43]	280	-	-
Uniyal et al. [44]	258.28	35.5	0.14
Kumar et al. [45]	264.59	-	0.12
Daher [38]	461.43	-	-
This work	**475.71**	**236.67**	**5.95**

values for infected RBCs are 2.01, 1.76, and 1.57°. The highest sensitivity, QF, and DA for the proposed sensor are 475.71, 236.82, and 5.95, respectively, which are enhanced very highly as compared to the performances of existing works, shown in Table 6.

Conclusion

The performance signature of the titanium dioxide (TiO_2)-2D nanomaterial-based surface plasmon resonance (SPR) sensor for detection of infected red blood cells (IRBCs) with *Plasmodium falciparum* is presented in this paper. The proposed structure consists of five layers, such as prism, silver (Ag), TiO_2, 2D nanomaterial, and sensing medium. Initially, an impact of TiO_2 in the SPR sensor is shown, demonstrating that 18% of sensitivity is improved with a TiO_2-based sensor (prism-Ag-TiO_2-sensing) compared to a conventional sensor. Moreover, the influence of 2D nanomaterials, such as MXene, graphene, BP, and MoS_2 is observed, resulting that MoS_2 is provided the maximum sensitivity compared to others. The respected 2D materials are improved the sensitivity by 11%, 4%, 10%, and 34% compared to the TiO_2-based sensor. Furthermore, the optimization of Ag, TiO_2, and MoS_2 thicknesses is presented by observing the maximum sensitivity. By using the optimized structure, we plotted the SPR curves and measured the sensitivity, quality factor (QF), and detection accuracy (DA) for the detection of IRBCs. The highest attained parameters are sensitivity of 475.71 °/RIU, QF of 236.67 RIU^{-1} and DA of 5.95 for the proposed sensor, which are far greater than performance of existing work. Therefore, the proposed SPR sensor can be utilized as high-performance carrier for IRBC detection, and accomplishes a new way for efficient photodetectors in the biomolecular field.

Author Contribution Conceptualization, Yesudasu Vasimalla, Himansu Shekhar Pradhan; data curation, formal analysis, investigation, Rahul Jashvantbhai Pandya, Kayam Sai Kumar; methodology, Twana Mohammed Kak Anwer, Md. Amzad Hossain, Ahmed Nabih Zaki Rashed; resources, software, Md. Amzad Hossain, Ahmed Nabih Zaki Rashed; supervision, validation, Yesudasu Vasimalla, Himansu Shekhar Pradhan; visualization, writing—original draft, Rahul Jashvantbhai Pandya, Yesudasu Vasimalla, Ahmed Nabih Zaki Rashed; writing—review editing.

Data Availability Not applicable.

Declarations

Ethics Approval Not applicable.

Consent to Participate Not applicable.

Consent for Publication Not applicable.

Conflict of Interest The authors declare no competing interests.

References

1. Nureye D, Assefa S (2020) Old and recent advances in life cycle, pathogenesis, diagnosis, prevention, and treatment of malaria including perspectives in Ethiopia. Sci World J 1–17. https://doi.org/10.1155/2020/1295381
2. Molina-Franky J, Cuy-Chaparro L, Camargo A, Reyes C, Gómez M, Salamanca D, Patarroyo M, Patarroyo M (2020) Plasmodium falciparum pre-erythrocytic stage vaccine development. Malar J 19(1);1–18. https://doi.org/10.1186/s12936-020-3141-z
3. Singh TI, Singh P, Karki B (2023) Early detection of chikungunya virus utilizing the surface plasmon resonance comprising a silver-silicon-PtSe2 multilayer structure. Plasmonics 1–8. https://doi.org/10.1007/s11468-023-01840-x
4. Karki B, Uniyal A, Srivastava G, Pal A (2023) Black phosphorous and Cytop nanofilm-based long-range SPR sensor with enhanced quality factor. J Sens. https://doi.org/10.1155/2023/2102915
5. Karki B, Ansari G, Uniyal A, Srivastava V (2023) PtSe2 and black phosphorus employed for sensitivity improvement in the surface plasmon resonance sensor. J Comput Electron 22(1):106–115. https://doi.org/10.1007/s10825-022-01975-w
6. Karki B, Uniyal A, Pal A, Srivastava V (2022) Advances in surface plasmon resonance-based biosensor technologies for cancer cell detection. Int J Opt. https://doi.org/10.1155/2022/1476254
7. Karki B, Jha A, Pal A, Srivastava V (2022) Sensitivity enhancement of refractive index-based surface plasmon resonance sensor for glucose detection. Opt Quant Ele 54(9):595. https://doi.org/10.1007/s11082-022-04004-z
8. Karki B, Vasudevan B, Uniyal A, Pal A, Srivastava V (2022) Hemoglobin detection in blood samples using a graphene-based surface plasmon resonance biosensor. Optik 270:169947. https://doi.org/10.1016/j.ijleo.2022.169947
9. Karki B, Ramya KC, Sandhya Devi RS, Srivastava V, Pal A (2022) Titanium dioxide, black phosphorus and bimetallic layer-based surface plasmon biosensor for formalin detection: numerical analysis. Opt Quant Ele 54(7):451. https://doi.org/10.1007/s11082-022-03875-6
10. Liu PY, Chin LK, Ser W, Chen H, Hsieh CM, Lee CH, Sung KB, Ayi T, Yap P, Liedberg B, Wang K, Bourouina T, Leprince-Wang Y (2016) Cell refractive index for cell biology and disease diagnosis: past, present and future. Lab Chip 16(4):634–644. https://doi.org/10.1039/c5lc01445j
11. Akpa Marcel A, Konan K, Tokou Z, Kossonou Y, Dion S, Kaduki K, Zoueu J (2019) Malaria-infected red blood cell analysis through optical and biochemical parameters using the transport of intensity equation and the microscope's optical properties. Sensors 19:3045. https://doi.org/10.3390/2Fs19143045
12. Bendib B, Bendib C (2018) Photonic crystals for malaria detection. J Biosens Bioelectron. https://doi.org/10.4172/2155-6210.1000257
13. Ragavan KV, Kumar S, Swaraj S, Neethirajan S (2018) Advances in biosensors and optical assays for diagnosis and detection of malaria. Biosens Bioelectron 105:188–210. https://doi.org/10.1016/j.bios.2018.01.037
14. Krampa F, Aniweh Y, Kanyong P, Awandare G (2020) Recent advances in the development of biosensors for malaria diagnosis. Sensors 20:799. https://doi.org/10.3390/2Fs20030799
15. Bilal M, Saleem M, Amanat S, Shakoor H, Rashid R, Mahmood A, Ahmed A (2015) Optical diagnosis of malaria infection in human plasma using Raman spectroscopy. J Biomed Opt 20(1):17002S. https://doi.org/10.1117/1.jbo.20.1.017002
16. Yan Q, Peng B, Su G, Cohan BE, Major TC, Meyerhoff ME (2011) Measurement of tear glucose levels with amperometric glucose biosensor/capillary tube configuration. Anal Chem 83:8341–8346. https://doi.org/10.1021/ac201700c
17. Dai X, Liang Y, Zhao Y, Gan S, Jia Y, Xiang Y (2019) Sensitivity enhancement of a surface plasmon resonance with tin selenide (SnSe) allotropes. Sensors 19(1):173. https://doi.org/10.3390/s19010173
18. Bochenkov VE, Frederiksen M, Sutherland DS (2013) Enhanced refractive index sensitivity of elevated short-range ordered nanohole arrays in optically thin plasmonic Au films. Opt Exp 21:14763. https://doi.org/10.1364/oe.21.014763
19. Wei PC, Bhattacharya S, He J, Neeleshwar S, Podila R, Chen YY, Rao AM (2016) The intrinsic thermal conductivity of SnSe. Nature 539(7627):1–3. https://doi.org/10.1038/nature19832
20. Zhao S et al (2015) Controlled synthesis of single-crystal SnSe nanoplates. Nano Res 8:288–295. https://doi.org/10.1007/s12274-014-0676-8
21. Homola J, Yee SS, Gauglitz G (1999) Surface plasmon resonance sensors: review. Sens Actuators B Chem 54:3–15. https://doi.org/10.1016/S0925-4005(98)00321-9
22. Kumar R et al (2020) Effect of silicon on sensitivity of SPR biosensor using hybrid nanostructure of black phosphorus and MXene. Superlattices Microstruct. 145:106591. https://doi.org/10.1016/j.spmi.2020.106591
23. Yotong S et al (2022) Temperature sensor based on surface plasmon resonance with TiO2-Au-TiO2 triple structure. Materials 15(21):7766. https://doi.org/10.3390/ma15217766
24. Gogotsi Y, Anasori B (2019) The rise of MXenes ACS nano 13(8):8491–8494. https://doi.org/10.1021/acsnano.9b06394
25. Shinde PV, Singh MK (2019) Synthesis, characterization, and properties of graphene analogs of 2D material. Fundam Sens Appl 2D Mater 91–143. https://doi.org/10.1016/B978-0-08-102577-2.00004-X
26. Chen P, Li N, Chen X, Ong WJ, Zhao X (2017) The rising star of 2D black phosphorus beyond graphene: synthesis, properties and electronic applications. 2D Mater 5(1):014002. https://doi.org/10.1088/2053-1583/aa8d37
27. Liao G et al (2019) Ag-based nanocomposites: synthesis and applications in catalysis". Nanoscale 11(15):7062–7096. https://doi.org/10.1039/c9nr01408j
28. Vijayalakshmi R, Rajendran V (2012) Synthesis and characterization of nano-TiO2 via different methods. Arch Appl Sci Res 4(2):1183–1190
29. Maurya JB, Prajapati YK (2020) Experimental demonstration of DNA hybridization using graphene based plasmonic sensor chip. J Lightwave Techn 38(18):5191–5198. https://doi.org/10.1109/JLT.2020.2998138
30. Nyamekye CKA et al (2019) Experimental analysis of waveguide-coupled surface-plasmon-polariton cone properties. Anal Chim Acta 1048:123–131. https://doi.org/10.1016/j.aca.2018.09.057
31. Vasimalla Y, Pradhan HS, Pandya RJ (2021) Sensitivity enhancement of the SPR biosensor for Pseudomonas bacterial detection employing a silicon-barium titanate structure. Appl Opt 60:5588–5598. https://doi.org/10.1364/AO.427499
32. Jabin M, Rana M, Al-Zahrani FA, Paul BK, Ahmed K, Bui FM (2022) Novel detection of diesel adulteration using silver-coated surface plasmon resonance sensor. Plasmonics 17:467–478. https://doi.org/10.1007/s11468-021-01540-4
33. Singh Y, Raghuwanshi SK (2021) Titanium dioxide (TiO2) coated optical fiber-based SPR sensor in near-infrared region with bimetallic structure for enhanced sensitivity. Optic 226:165842. https://doi.org/10.1016/j.ijleo.2020.165842
34. Pal S et al (2020) Sensitive detection using heterostructure of black phosphorus, transition metal di-chalcogenides and MXene in SPR sensor. Appl Phys A 126(10):809. https://doi.org/10.1007/s00339-020-03998-1
35. Szunerits S et al (2013) Recent advances in the development of graphene-based surface plasmon resonance (SPR) interfaces. Anal Bioanal Chem 405:1435–1443. https://doi.org/10.1007/s00216-012-6624-0

36. Vasimalla Y, Pradhan HS, Pandya RJ (2020) SPR performance enhancement for DNA hybridization employing black phosphorus, silver, and silicon. Appl Opt 59(24):7299–7307. https://doi.org/10.1364/ao.397452
37. Cai H et al (2022) Performance enhancement of SPR biosensor using graphene–MoS2 hybrid structure. Nanomaterials 12(13):2219. https://doi.org/10.3390/nano12132219
38. Daher MG (2023) Highly sensitive detection of infected red blood cells (IRBCs) with plasmodium falciparum using surface plasmon resonance (SPR) nanostructure. Opt Quant Ele 55(3):199. https://doi.org/10.1007/s11082-022-04466-1
39. Jia Y, Li Z, Wang H, Saeed M, Cai H (2020) Sensitivity enhancement of a surface plasmon resonance sensor with platinum diselenide. Sensors 20(1):131. https://doi.org/10.3390/s20010131
40. Pal S, Prajapati YK, Saini JP (2020) Infuence of grapheme'chemical potential on SPR biosensor using ZnO for DNA hybridization. Opt Rev 27:57–64. https://doi.org/10.1007/s10043-019-00564-w
41. Taya SA, Al-Ashi NE, Ramahi OM, Colak I, Amiri IS (2021) Surface plasmon resonance-based optical sensor using a thin layer of plasma. J Opt Soc Am B 38:2362–2337. https://doi.org/10.1364/JOSAB.420129
42. Mudgal N, Saharia A, Agarwal A, Ali J, Yupapin P, Singh G (2020) Modeling of highly sensitive surface plasmon resonance (SPR) sensor for urine glucose detection. Opt Quantum Electron 52(6):1–14. https://doi.org/10.1007/s11082-020-02427-0
43. Pal A, Jha A (2021) A theoretical analysis on sensitivity improvement of an SPR refractive index sensor with graphene and barium titanate nanosheets. Optik 231:166378. https://doi.org/10.1016/j.ijleo.2021.166378
44. Uniyal A, Chauhan B, Pal A (2022) Bi-metallic films of gold, MXene, and graphene nano film-based surface plasmon resonance sensor for malaria detection: a numerical analysis. https://doi.org/10.21203/rs.3.rs-1766754/v1
45. Kumar R, Pal S, Prajapati YK, Kumar S (2022) Saini J P (2022) Sensitivity improvement of a MXene- immobilized SPR sensor with Ga-doped-ZnO for biomolecules detection. IEEE Sens J 22(7):6536–6543. https://doi.org/10.1109/JSEN.2022.3154099

Authors and Affiliations

Yesudasu Vasimalla[1] · Himansu Shekhar Pradhan[2] · Rahul Jashvantbhai Pandya[3] · Kayam Saikumar[4] · Twana Mohammed Kak Anwer[5] · Ahmed Nabih Zaki Rashed[6,7] · Md. Amzad Hossain[8]

✉ Ahmed Nabih Zaki Rashed
ahmed_733@yahoo.com

✉ Md. Amzad Hossain
mahossain.eee@gmail.com

Yesudasu Vasimalla
vasimalladasu@gmail.com

Himansu Shekhar Pradhan
hsp@nitw.ac.in

Rahul Jashvantbhai Pandya
rpandya@iitdh.ac.in

Kayam Saikumar
saikumarkayam4@ieee.org

Twana Mohammed Kak Anwer
twana.anwar1@su.edu.krd

[1] Department of Electronics and Communication Engineering, Koneru Lakshmaiah Educational Foundation (KLEF), Vaddeswaram, Andhra Pradesh 522302, India

[2] National Institute of Technology, Warangal, Telangana 506004, India

[3] Department of Electrical Engineering, Indian Institute of Technology Dharwad, Dharwad, Karnataka, India

[4] School of Engineering, Department of CSE, Malla Reddy University, Maisammaguda, Dulapally, Hyderabad, Telangana 500043, India

[5] Department of Physics, College of Education, Salahaddin University-Erbil, 44002 Erbil, Kurdistan Region, Iraq

[6] Electronics and Electrical Communications Engineering Department, Faculty of Electronic Engineering, Menoufia University, Menouf 32951, Egypt

[7] Department of VLSI Microelectronics, Institute of Electronics and Communication Engineering, Saveetha School of Engineering, SIMATS, Chennai 602105, Tamil Nadu, India

[8] Department of Electrical and Electronic Engineering, Jashore University of Science and Technology, Jashore 7408, Bangladesh